Unraveling the conundrum of river response to rising sea level from laboratory to field. Part I. Laboratory experiments

GARY PARKER[a], TETSUJI MUTO[b], YOSHIHISA AKAMATSU[c], WILLIAM E. DIETRICH[d] and J. WESLEY LAUER[e]

[a]*Dept. of Civil and Environmental Engineering and Dept. of Geology, University of Illinois, Hydrosystems Laboratory, 205 N. Mathews, Urbana Illinois 61801 USA.*
[b]*Faculty of Environmental Studies, Nagasaki University, 1-14 Bunkyomachi, Nagasaki 852-8521, Japan*
[c]*Department of Environmental Science and Technology, Tokyo Institute of Technology 4259, Nagatsuda-cho, Midori-ku, Yokohama-shi, Kanagawa, 226-8502, Japan*
[d]*Department of Earth and Planetary Science, University of California Berkeley, CA 94720-4767 USA*
[e]*St. Anthony Falls Laboratory, University of Minnesota, 2 3rd St. SE, Minneapolis, MN 55141 USA.*

ABSTRACT

The most recent deglaciation resulted in a global sea level rise of some 120 m over approximately 12000 years. In this Part I of two parts, a moving boundary numerical model is developed to predict the response of rivers to this rise. The model was motivated by experiments at small-scale, which have identified two modes describing the transgression of a river mouth: autoretreat without abandonment of the river delta (no sediment starvation at the topset-foreset break) and sediment-starved autoretreat with abandonment of the delta. In the latter case transgression is far more rapid, and its effects are felt much farther upstream of the river mouth. The moving boundary numerical model is checked against experiments. The generally favorable results of the check motivatate adaptation of the model to describe to describe the response of the much larger

Fly-Strickland River system, Papua New Guinea to Holocene sea level rise. This is done in the companion paper, Part II.

Keywords rivers, deltas, transgression, sea level, autoretreat

INTRODUCTION

The last deglaciation resulted in a Pleistocene-Holocene global sea level rise of some 120 m. Nearly all this rise was realized in a 12000 period between 18000 and 6000 years BP. The sea level curve of Bard *et al.* (1996) documenting this rise is given as Fig. 1. Sea level rise likely had a dramatic effect on rivers near their mouths.

The effect of eustatic sea level rise depends on the tectonic setting. Along uplifting active margins, the rate of sea level rise relative to the margin itself was less than that predicted by the Bard Curve of Fig. 1. Along slowly subsiding passive margins, however, the full brunt of Pleistocene-Holocene sea level rise was felt.

The passive margin of the East Coast of the US provides an example. The coastline from New Jersey to North Carolina shows a series of embayments or estuaries, including Delaware Bay, Chesapeake Bay and Albemarle Sound (Fig. 2.) Evidently the mouths of the rivers flowing into this region were drowned by sea level rise (e.g. Bratton *et al*., 2003). The margin of the northern Gulf of Mexico near the Mississippi River delta, on the other hand, presents a very different picture (Fig. 3). Rather than forming an embayment, the Mississippi River forms a delta which protrudes into the Gulf of Mexico. Evidently the

Mississippi River was able to resist drowning due to sea level rise, or was able to recover from it more quickly than the rivers of Fig. 2.

Why would rivers along the same margin of the same continent respond so differently to Post-glacial Pleistocene-Holocene sea level rise? A key feature is likely to be sediment supply. Most of the rivers of Fig. 2 flow from the Appalachian Mountains, a geologically old formation that no longer uplifts and produces little sediment. The Mississippi River, on the other hand, drains a huge area that includes much of the geologically younger Rocky Mountains. Evidently under the right conditions a sufficiently high sediment supply can prevent river mouths from being drowned due to sea level rise, or at least allow more rapid recovery after sea level stabilizes.

This paper (Part I) and its companion paper (Part II) are devoted to a study of the effect of sea level rise on rivers, not only at their mouths but farther upstream.

GUIDE TO THE PAPERS

This paper and its companion paper are long, and freely use the language of mathematics. The goal, however, is to explain the process of river response to sea level rise in physical terms. With this in mind, a brief summary is given as a guide.

The story begins in this paper with the small-scale experiments of Muto (2001) on the effect of sea level rise on one-dimensional alluvial deltas. Under conditions of constant sea level, or stillstand, the model river developed an

upward-concave long profile and prograded into ever-deeper water at an ever-decreasing, but always finite speed. A different picture emerged when sea level was raised at a constant speed. Initially both the delta topset-foreset break and toe (foreset-subaqueous basement break) continued to prograde seaward. If sea level rise were continued for a sufficiently long time, however, at some point the delta topset-foreset break would start to transgress landward, even though the delta toe continued to move seaward. Muto and Steel (1992, 1997) called this process "autoretreat." With a further continuation of sea level rise, at some point the sediment delivery to the topset-foreset break would drop to zero. Muto (2001) referred to this as the point of "autobreak," after which the delta front would be abandoned, and the shoreline would go into a rapid transgression, here termed "sediment-starved autoretreat." The result of this rapid transgression would be the formation of an embayment reminiscent of those shown in Fig. 2. The patterns observed in the experiments of Muto (2001) are summarized in Fig. 4.

The experiments motivate the following question. Do the experiments of Muto (2001) and the observed phenomenon of autoretreat shed light on the response of rivers to Pleistocene-Holocene sea level rise? Blum and Törnqvist (2000) note that the issue of fluvial response to sea level change has been hotly debated, with some authors suggesting that the effects were likely localized near river mouths and others arguing that the effects extended far upstream. In the same paper they argue for the importance of modeling in the study of the problem (see also Paola, 2000).

A number of peculiarities of the physical modeling of Muto (2001) ensure that the results cannot be directly applied to the field. Numerical modeling, however, can serve as a powerful bridge between laboratory experiments and rivers. A numerical model can be thought of as a chest of drawers filled with information. The contents of some of the drawers must be specific to the setting, i.e. either experimental or field. The contents of most of the drawers, and the overall structure of the chest, however, do not change. Such a model allows for effective upscaling of experimental results, as well as a reasonable means for determining whether experimental results have field applicability.

Here the basic structure of a numerical model is developed in the context of the experiments of Muto (2001). The model is verified with the aid of experiments in Part I. The model is then modified and adapted for application to large, low-slope sand-bed rivers in Part II. It is applied therein to the Fly-Strickland River system of Papua New Guinea (Dietrich *et al.*, 1999). The results of the modeling are combined with field information to demonstrate the following: a) The Fly-Strickland River System likely did go into autoretreat during Pleistocene-Holocene sea level rise, and is still recovering from the effects of this rise, and b) the effect of sea level rise likely propagated many hundreds of km upstream, to the point of causing migration of a gravel-sand transition.

EXPERIMENTS OF MUTO

Muto (2001) considered the simple one-dimensional configuration sketched in Fig. 5. Water and sediment were introduced into a narrow channel with an

inerodible basement. The basement had constant slope S_b and slope angle $\theta_{base} = \tan^{-1}(S_b)$. The basement slope was chosen to be sufficiently steep so that the sediment was transported over it under below-capacity conditions (partial exposure of the inerodible bed), with negligible sediment deposition. The basement thus served as a simple model for a bedrock channel. Ponded water was maintained at the downstream end, and was allowed to rise at the constant rate $\dot{\xi}$. This ponding forced the flow to decelerate and the sediment to deposit out on the bed, forming an alluvial topset and an avalanching foreset (Figs. 4, 5). The transition from a bedrock reach over which sediment was transport under below-capacity conditions to an alluvial reach over which sediment was transport at capacity defined a moving boundary.

Before enumerating the experimental conditions in detail, it is useful to study Fig. 4, which shows the delta configuration at the end of one of the experiments. It can be seen in the image that the both the shoreline (topset-foreset break) and the delta toe (foreset-subaqueous basement break) first prograded (regressed). As sea level rise continued, however, the shoreline started to move landward, or regress, even as the delta toe continued to prograde. This change marked the start of autoretreat. With continued sea level rise, the delta front was eventually abandoned, and the shoreline rapidly transgressed with vanishing sediment delivery to the delta. Muto (2001) has termed the start of this process "autobreak." The rapid transgression after autobreak is here termed "sediment-starved autoretreat." During the course of the experiments, the bedrock-alluvial transition migrated upstream (Fig. 4).

The experiments of Muto (2001) were conducted in a narrow tank with a length of 2 m and a depth of 1 m. The width of the tank was either 5 or 10 mm for the experiments. This configuration allowed for a simple one-dimensional delta without complications in the transverse direction. (Muto and Steel, 2001, have, however, demonstrated the concept of autoretreat in the case of two-dimensional deltas with transverse flare.) The sediment used in the experiments was a uniform fine quartz sand with a median geometric mean size D of 0.212 mm, a geometric standard deviation of 1.24 and a specific gravity near 2.65.

The 29 experiments in Table 1 of Muto (2001) are considered here. Basement slope angle θ_{base} varied from 11.9° to 31.2°; the angle of repose θ_r of the sediment was found to be near 35°. Water discharge per unit width q_w took one of the two values 2.18 cm^2/s and 4.36 cm^2/s. Volume sediment feed per unit width q_{psf} (sediment + pores) ranged from 0.297 cm^2/s to 1.093 cm^2/s. The rate of base level rise $\dot{\xi}$, which was held constant for the duration of each experiment, varied from 0.126 mm/s to 0.387 mm/s. As can be seen in Fig. 4, a small amount of black carborundum powder was occasionally allowed to deposit to help visualize the structure of the deposit.

Any attempt at a mechanistic numerical model of the experiments of Muto (2001) requires an appropriate sediment transport relation. The experiments are, however, peculiar in this regard. More specifically, a) volume concentration of sediment in the slurry fed into the flume was very high, i.e. on the order of 10 percent and b) flow depth was very low, i.e. on the order of 1 mm. As a result, none of the many existing relations for transport of sand at either field or

laboratory scale (see e.g. Brownlie, 1981 for a compendium) were applicable to the data.

It might then be argued that because the sediment transport observed in the experiments fitted no existing transport relation, and specifically no relation known to be applicable to field-scale rivers, the experiments are of no value in explaining field-scale river response to sea level rise. This is not the case at all. The experiments can be used to develop a crude but reasonable empirical sediment transport relation, which can in turn be used in the development of a numerical model of response to sea level rise. Application of the numerical model to field-scale rivers then requires (among other modifications) a simple replacement of the empirical sediment transport relation appropriate for the experiments with a relation appropriate for natural rivers.

The flow discharge per unit width is denoted here as q_w; the volume sediment transport rate per unit width (sediment + pores) is denoted as q_{ps}. Muto (2001) recorded the bed slope angle θ_u at the upstream end of the alluvial deposit, where the transition from bedrock to alluvial conditions is made. The bed slope $S_u = \tan(\theta_u)$ thus corresponds to the slope at which the unit sediment feed rate q_{psf} is just transported at capacity by the unit flow discharge q_w. With this in mind a simple dimensionless relation of the following form is hypothesized for sediment transport. Let S denote the local bed slope. The sediment transport relation takes the form

$$\frac{q_{ps}}{q_w} = \alpha S^n \qquad (1a)$$

where α is a dimensionless coefficient and n is an exponent. Based on the data of Muto (2001), the following values of α and n were determined by regression, as shown in Fig. 6;

$$\alpha = 12.3\,, \quad n = 2.24 \qquad (1b,c)$$

The coefficient of correlation R^2 is given in the figure. While the scatter in Fig. 6 is considerable and the form of Eq. (1a) is purely empirical and specific to the experiments in question, the relation captures the essential trends of sediment transport: increasing bed slope and increasing flow rate lead to an increase in the sediment transport rate.

The depths of flow in the experiments were on the order of one or two mm. While it was not possible to calculate precise values of the Froude numbers of the flow, estimates indicated that the flow was invariably in the range of either supercritical flow or subcritical flow with a Froude number not far below unity. As a result, backwater effects could be neglected in analyzing the experiments.

NUMERICAL FORMULATION AND IMPLEMENTATION: EXPERIMENTAL SCALE

The numerical model described below is a descendant of the work of Swenson *et al.* (2000) and Kostic and Parker (2003a,b). These models allow for two moving boundaries; the topset-foreset break (shoreline) and the foreset-bottomset break (foreset-subaqueous basement break in the present case). The present analysis also allows a third moving boundary, i.e. the bedrock-alluvial transition point shown in Figs. 4 and 5.

Parameters The key parameters of the analysis are defined as follows and illustrated in Fig. 5. Where x denotes downstream distance and t denotes time, $x = s_{ba}(t)$ denotes the position of the bedrock-alluvial break, $x = s_s(t)$ denotes the position of the topset-foreset break (shoreline) and $x = s_{sb}(t)$ denotes the position of the foreset-subaqueous basement break. These three positions describe the moving boundaries of the problem. In addition, η denotes alluvial bed elevation, η_{base} denotes elevation of the bedrock basement and S_b denotes the slope of the bedrock basement on which the sediment deposits, which was constant in the case of the experiments of Muto (2001). The slope of avalanching onto the foreset is denoted as S_{fore}, where S_{fore} must satisfy the condition $S_{fore} > S_b$ (Figs. 4 and 5). In the experiments of Muto (2001) S_a was equal to the tangent of measured the angle of repose θ_r of about 35°. The volume sediment transport rate per unit width (including pores) is denoted as q_{ps}. Base level (elevation of standing water at the downstream end) is denoted as ξ. The time rate of base level rise is denoted as $\dot{\xi}$; this parameter was held constant in the case of the experiments of Muto (2001). Alluvial bed slope S is given as

$$S = -\frac{\partial \eta}{\partial x} \qquad (2)$$

Sediment conservation The Exner equation of sediment conservation can be written as

$$\frac{\partial \eta}{\partial t} = -\frac{\partial q_{ps}}{\partial x} \qquad (3)$$

where

$$q_{ps} = \frac{q_s}{(1-\lambda_p)} \tag{4}$$

In the above relation q_{ps} denotes the volume sediment transport rate per unit width including both sediment and pores, q_s denotes the volume transport rate per unit width of sediment only and λ_p denotes the porosity of the bed deposit. In the experiments under consideration the porosity was near 0.5.

Upstream conditions The delta builds out over a set basement with elevation profile $\eta_{base}(x)$ and constant slope S_b. The alluvial zone of the delta begins at the bedrock-alluvial break with an elevation equal to that of the basement, and ends at the elevation of the standing water. The boundary conditions on (1) at the upstream end of the alluvial zone are a sediment feed condition;

$$q_{ps}\Big|_{x=s_{ba}} = q_{psf} \tag{5}$$

where q_{psf} denotes the feed value of q_{ps}, and a continuity condition matching the bedrock zone smoothly with the alluvial zone;

$$\eta_{ba}(t) \equiv \eta[s_{ba}(t), t] = \eta_{base}[s_{ba}(t)] \tag{6}$$

Equation (5) is further reduced by taking the time derivative, resulting in the relation

$$\dot{s}_{ba} = -\frac{1}{S_b - S_{aba}} \frac{\partial \eta}{\partial t}\Big|_{s_{ba}} \tag{7a}$$

where the dot denotes a time derivative, S_{aba} denotes the upstream alluvial bed slope at the bedrock-alluvial transition and S_b denotes the basement slope;

$$S_{aba} = -\left.\frac{\partial \eta}{\partial x}\right|_{s_{ba}}, \quad S_b = -\frac{\partial \eta_{base}}{\partial x} \qquad (7b,c)$$

Interpretation The physical meaning of (7a) can be explained as follows. In order for sediment to be transported under below-capacity conditions upstream of the bedrock-alluvial break, it is necessary for S_b to exceed the bed slope associated with at-capacity transport. Since the sediment fed in from upstream first forms an alluvial bed at $x = s_{ba}$, the alluvial slope S_{aba} at this point is the slope associated with the sediment feed rate q_{psf}. Thus in order for the transition to exist it is necessary for S_b to exceed S_{aba}. As long as this condition is satisfied, (7a) ensures that:

- under conditions of bed aggradation at the bedrock-alluvial transition ($\partial\eta/\partial t > 0$ at $x = s_{ba}$) the alluvium onlaps onto the bedrock and the bedrock-alluvial transition moves upstream, as illustrated in Fig. 7; and
- under conditions of bed degradation at the bedrock-alluvial transition ($\partial\eta/\partial t < 0$ at $x = s_{ba}$) the alluvium is swept seaward and the bedrock-alluvial transition moves downstream.

Shoreline condition A continuity condition similar to (5) holds at the shoreline, where the water surface of the river is set equal to the elevation of standing water. Denoting river depth as H(x, t), the condition becomes

$$\eta[s_s(t), t] + H[s_s(t), t] = \xi_i + \dot{\xi} t \qquad (8a)$$

where ξ_i denotes an initial base level elevation. In the case of the experiments of Muto (2001), flow depth is so small (on the order of 1 mm) that (8a) can be accurately approximated to

$$\eta_s \equiv \eta[s_s(t), t] = \xi_i + \dot{\xi} t \qquad (8b)$$

Taking the time derivative of the above relation, it is found that

$$\frac{d\eta_s}{dt} = \dot{\xi} \qquad (8c)$$

Interpretation Condition (8c) pins the location of the topset-foreset break to the shoreline. The topset-foreset break moves up or down in precise consonance with sea level. The condition proves to be quite accurate in the context of the experiments of Muto (2001), but will be relaxed in considering field-scale rivers.

Conditions at the foreset-basement break Beyond the end of the fluvial topset zone the sediment forms a subaqueous foreset that progrades at slope S_a by avalanching. The bed profile on the foreset is

$$\eta = \eta_s - S_{fore}(x - s_s) \qquad (9)$$

over the zone $s_s < x < s_{sb}$. In the experiments of Muto (2001) all of the sediment delivered to the topset-foreset break was deposited on the foreset, with no bottomset deposition (Fig. 5). One boundary condition at the foreset-subaqueous basement break is thus

$$q_{ps}\Big|_{x=S_{sb}} = 0 \qquad (10)$$

In addition to the above relation, the following continuity condition holds at the foreset-basement break;

$$\eta[s_{sb}(t), t] = \eta_s - S_{fore}(s_{sb} - s_s) = \eta_{base}[s_{sb}(t)] \qquad (11)$$

The above equation can be differentiated with respect to time and reduced with (8c) to yield the result

$$\dot{s}_{sb} = \frac{S_{fore}}{S_{fore} - S_b}\dot{s}_s + \frac{1}{S_{fore} - S_b}\dot{\xi} \qquad (12)$$

Interpretation Equation (12) is most easily understood by considering the case of a delta prograding over a horizontal bed under conditions of constant sea level ($S_b = 0$, $\dot{\xi} = 0$) in which case (12) reduces to

$$\dot{s}_b = \dot{s}_s \qquad (13)$$

Under the stated conditions the foreset-basement break moves at the same speed as the topset-foreset break (shoreline), as illustrated in Fig. 8a. A comparison of (12) and Fig. 8b shows that a subaqueous basement that becomes deeper offshore ($S_b > 0$) and rising base level ($\dot{\xi} > 0$) act to cause the foreset-subaqueous basement break to prograde outward faster than the topset-foreset break.

Shock condition across the foreset If the delta is prograding outward, the speed of migration $\dot{s}_s$ of the shoreline is constrained by a shock condition that can be derived by integrating (3) across the foreset, i.e. from $x = s_s$ to $x = s_{sb}$. The term $\partial\eta/\partial t$ on the foreset is obtained by differentiating (9) with respect to time and reducing with (8c), yielding the result

$$\frac{\partial \eta}{\partial t} = \dot{\xi} + S_{fore}\dot{s}_b \qquad (14a)$$

Integrating (3) from s_s to s_{sb} and reducing with (10) and (14a) yields the shock condition

$$\dot{s}_s = \frac{1}{S_{fore}}\left(\frac{q_{pss}}{s_{sb} - s_s} - \dot{\xi}\right) \qquad (14b)$$

where

$$q_{pss} \equiv q_{ps}[s_s(t), t] \tag{14c}$$

describes the rate of sediment delivery to the topset-foreset break (Swenson *et al*., 2000; Kostic and Parker, 2003a).

Interpretation The height of the foreset $\Delta\eta$ is given as

$$\Delta\eta = S_{fore}(s_{sb} - s_s) \tag{16a}$$

(Fig. 7a), so that (14b) can be rewritten as

$$\dot{s}_s = \frac{q_{pss}}{\Delta\eta} - \frac{\dot{\xi}}{S_{fore}} \tag{16b}$$

In the absence of sea level rise, (16b) reduces to the simple form

$$\dot{s}_s \Delta\eta = q_{pss} \tag{16c}$$

That is, the delta front progrades (regresses) in consonance with the filling of the front by sediment delivered to the topset-foreset break, as illustrated in Fig. 8a. It is seen from (16b) and Fig. 8b that rising sea level and a subaqueous basement that slopes seaward ($S_b > 0$) reduce the speed of delta progradation. If sea level rises at a sufficiently high rate the effect of sediment delivery to the delta front can be counteracted, and the delta front can move landward (transgress). This transgression defines the condition of autoretreat.

Conditions for sediment starvation at the shoreline Equation (14b) adequately describes the regression or transgression of the topset-foreset break as long as there is sediment supply to the delta front. The experiments of Muto (2001) demonstrate, however, that if sea level rise at a constant rate is sustained for a sufficiently long time, the rate of sediment delivery eventually drops to zero and the delta front becomes starved of sediment. Under such conditions the

shoreline enters a mode of rapid transgression here termed "sediment-starved autoretreat." Under such condition the boundary condition of (14b) must be replaced with the condition

$$q_{ps}[s_s(t), t] = 0 \qquad (17)$$

It is now possible to specify regimes for delta development.

1. The case ($\dot{s}_s > 0, \dot{s}_{sb} > 0$) corresponds to a prograding delta, i.e. one for which both the shoreline and the foreset-basement break undergo regression.
2. The case ($\dot{s}_s < 0, \dot{s}_{sb} > 0$) corresponds to a delta with a shoreline undergoing autoretreat (transgression) but a foreset-basement break that continues to prograde (regress). The case of autobreak is reached when $\dot{s}_{sb}$ declines to zero and the delta toe can no longer prograde due to sediment starvation.
3. The case ($s_s < 0$, $s_{sb} = 0$) corresponds to sediment-starved autoretreat, for which the shoreline retreats (transgresses) and the subaqueous foreset becomes a dormant relict.

For cases 1 and 2 the appropriate downstream conditions at the shoreline are (8c) and (14b). For case 3 the appropriate conditions at the shoreline become (8c) and (17).

Initial conditions The initial bed consists of a very short alluvial reach of specified constant slope, followed by a commensurately short foreset. The parameters s_{ba} and s_s are assumed to take the initial values $s_{ba} = 0$, $s_s = s_{si}$, so

that the initial length of the fluvial zone is s_{si}. The initial elevation of the shoreline is taken to be $\eta_{si} = \xi_i = 0$, and the initial bed profile of the fluvial zone is

$$\eta(x,0) = \eta_i(x) = S_{fi}(s_{si} - x), \quad 0 < x < s_{si} \tag{18a}$$

where S_{fi} denotes the (constant) initial bed slope of the fluvial topset zone. The initial profile of the subaqueous delta is given as

$$\eta(x,0) = -S_{fore}(x - s_{si}), \quad s_{si} < x < s_{sbi} \tag{18b}$$

where s_{sbi} denotes the initial position of the foreset-subaqueous bottomset break. The initial height of the foreset is taken to be $\Delta\eta_i$, so that s_{sbi} and s_{si} are related by the geometric condition illustrated in Fig. 8a;

$$s_{sbi} = s_{si} + \frac{\Delta\eta_i}{S_{fore}} \tag{18c}$$

The basement profile $\eta_{base}(x)$ must thus have slope S_b, attain the elevation $S_{fi}s_{si}$ at x = 0 and attain the elevation $-\Delta\eta_i$ at $x = s_b$ (Fig. 8). This condition imposes a relation between $\Delta\eta_i$ and S_b;

$$\Delta\eta_i = \frac{(S_b - S_{fi})s_{si}}{1 - \dfrac{S_b}{S_{fore}}} \tag{19}$$

The basement profile, which is assumed to be invariant, is then given as

$$\eta_{base}(x) = S_{fi}s_{si} - S_b x \tag{20}$$

Flow of the calculation The calculation proceeds as follows. The alluvial domain is discretized into N+1 nodes, where the last of these is located at the shoreline. For a given bed configuration S and q_{ps} are computed on the alluvial zone from (2) and (1), respectively. The condition (5) is imposed in terms of an upstream ghost node. The bed elevation one time step later is then

computed from a discretized version of (3). The migration of the bedrock-alluvial break is computed from (7a). In the event that $q_{ss} > 0$, i.e. there is supply of sediment to the shoreline, the migration of the shoreline and foreset-basement break are computed from (14b) and (12), respectively.

The aggradational nature of the problem forces q_s to decline in x from the bedrock-alluvial break s_{ba} to the shoreline s_s. As the calculation proceeds, it can be expected that the shoreline value q_{pss} eventually drops to zero, indicating autobreak and the onset of sediment-starved autoretreat. In a discretized calculation, this is first realized in terms of a negative value of q_{ss}. From this point on conditions (12) and (14b) must be abandoned. The foreset-subaqueous basement break is no longer allowed to move, and the movement of the topset-foreset break is now described by (17) instead of (14b). The motion of the shoreline can be described by interpolating upstream from the current point s_s at which $q_{ss} < 0$ to a new value of s_s at which q_{ss} equals zero and (17) is satisfied.

Transformation to moving boundary coordinates The above problem is solved on a deforming grid using the coordinate transformation

$$\bar{x} = \frac{x - s_{ba}(t)}{s_s(t) - s_{ba}(t)}, \quad \bar{t} = t \tag{21a,b}$$

Note that the parameter $\bar{x}$ is defined so that $\bar{x} = 0$ at the bedrock-alluvial transition and $\bar{x} = 1$ at the shoreline (topset-foreset break). Equations (3), (5), (7a), (8b), (12), (14b) and (17) transform to the respective forms

$$\frac{\partial \eta}{\partial \bar{t}} - \frac{\left[\bar{x}\dot{s}_s + (1-\bar{x})\dot{s}_{ba}\right]}{s_s - s_{ba}} \frac{\partial \eta}{\partial \bar{x}} = -\frac{1}{s_s - s_{ba}} \frac{\partial q_{ps}}{\partial \bar{x}} \tag{22}$$

$$q_{ps}\Big|_{\bar{x}=0} = q_{psf} \tag{23}$$

$$\dot{s}_{ba} = -\frac{1}{S_b}\left.\frac{\partial \eta}{\partial \bar{t}}\right|_{\bar{x}=0} \tag{24}$$

$$\eta[1,\bar{t}] = \dot{\xi}\bar{t} \tag{25}$$

$$\dot{s}_{sb} = \frac{1}{S_{fore} - S_b}\left(S_{fore}\dot{s}_s + \dot{\xi}\right) \tag{26}$$

$$\dot{s}_s = \frac{1}{S_{fore}}\left(\frac{q_{ps}(1,\bar{t})}{s_{sb} - s_s} - \dot{\xi}\right) \tag{27}$$

$$q_s[1,\bar{t}] = 0 \tag{28}$$

Equation (24) can be further reduced; evaluating (22) at $\bar{x} = 0$ and substituting the results into (24),

$$\dot{s}_{ba} = \frac{1}{S_b - S_{aba}}\frac{1}{s_s - s_{ba}}\left.\frac{\partial q_{ps}}{\partial \bar{x}}\right|_{\bar{x}=0} \tag{29}$$

Discretization The alluvial domain $0 \le \bar{x} \le 1$ is discretized into N intervals, each with length

$$\Delta\bar{x} = \frac{1}{N} \tag{30}$$

bounded by N+1 nodes i = 1..N+1. The upstream and downstream elevations are η_1 and η_{N+1}, respectively. The load nodes are staggered a distance of 0.5 $\Delta\bar{x}$ from the elevation nodes, as illustrated in Fig. 9. The load node 1 corresponds to a ghost node where the sediment feed rate q_{psf} is specified. Equation (22) is discretized to

$$\eta_i\big|_{\bar{t}+\Delta\bar{t}} = \eta_i\big|_{\bar{t}} - \left[\bar{x}_i\dot{s}_s + (1-\bar{x}_i)\dot{s}_{ba}\right]S_i\Delta\bar{t} + \frac{q_{ps,i} - q_{ps,i+1}}{\Delta\bar{x}}\frac{\Delta\bar{t}}{s_s - s_{ba}} \tag{31}$$

where $\Delta\bar{t}$ denotes the time step, all terms on the right-hand side of (31) are evaluated at time $\bar{t}$ and bed slope S_i at the ith node is discretized as

$$S_i = \begin{cases} \dfrac{1}{s_s - s_{ba}} \dfrac{\eta_{i-1} - \eta_{i+1}}{2\Delta\bar{x}}, & i = 2..N \\ \dfrac{1}{s_s - s_{ba}} \dfrac{\eta_i - \eta_{i+1}}{\Delta\bar{x}}, & i = 1 \end{cases} \tag{32}$$

That is, (31) is used to calculate the change in bed elevation over one time step $\Delta\bar{t}$ for nodes i = 1..N. The change in bed elevation at node i = N+1 is given by the boundary condition (25) . The sediment transport rate at node 1 is computed via (23);

$$q_{ps,1} = q_{psf} \tag{33}$$

The sediment transport rates $q_{ps,i}$, i = 2..N+1 are computed as functions of slope $\hat{S}_i$ according to (1), where

$$\hat{S}_i = \frac{1}{s_s - s_{ba}} \frac{\eta_{i-1} - \eta_i}{\Delta\bar{x}} \tag{34}$$

Note that according to (32) a central difference scheme is used to compute bed slope S_i at all nodes except node 1 in (31), whereas the backward difference scheme of (33) is used to compute the bed slope $\hat{S}_i$ employed in the computation of the bedload transport rate $q_{ps,i}$ at the ith node.

Conditions (29), (27) and (26) are easily implemented in discretized form to determine $\dot{s}_{ba}$, $\dot{s}_s$ and $\dot{s}_{sb}$. For example, (29) and (27) discretize to the following respective forms:

$$\dot{s}_{ba} = \frac{1}{S_b - S_1} \frac{1}{s_s - s_{ba}} \frac{q_{ps,1} - q_{psf}}{\Delta\bar{x}} \tag{34}$$

$$\dot{s}_s = \frac{1}{S_a}\left(\frac{q_{ps,N+1}}{s_{sb}-s_s} - \dot{\xi}\right) \tag{35}$$

Once s_{ba}, s_s, s_{sb}, $\dot{s}_{ba}$, $\dot{s}_s$ and $\dot{s}_{sb}$ are all known at a given time $\bar{t}$, the values for s_{ba}, s_s and s_{sb} at the next time step are computed as

$$s_{ba}\Big|_{\bar{t}+\Delta\bar{t}} = s_{ba} + \dot{s}_{ba}\Delta\bar{t} \tag{36a}$$

$$s_s\Big|_{\bar{t}+\Delta\bar{t}} = s_s + \dot{s}_s\Delta\bar{t} \tag{36b}$$

$$s_{sb}\Big|_{\bar{t}+\Delta\bar{t}} = s_{sb} + \dot{s}_{sb}\Delta\bar{t} \tag{36c}$$

Condition (28) is implemented via interpolation. It is seen from (1) that the sediment supply rate to the shoreline q_{pss} vanishes when the bed slope vanishes there. Suppose that at some stage in the calculation the shoreline bed slope $\hat{S}_{N+1}$ barely becomes negative. As long as the time step is sufficiently short $\hat{S}_N$ can be expected to be positive. As a result the position $s_{s,noload}$ corresponding to vanishing load at which (28) is satisfied can be estimated as

$$s_{s,noload} = s_{ba} + (s_s - s_{ba})\left[\bar{x}_N - \frac{\Delta\bar{x}}{\hat{S}_{N+1}-\hat{S}_N}\hat{S}_N\right] \tag{35}$$

The value $s_{s,noload}$ is used as the value of s_s in the next time step, and η_i for the next time step is computed via (31) using the following estimate of $\dot{s}_s$;

$$\dot{s}_s = \frac{s_{s,noload} - s_s}{\Delta\bar{t}} \tag{36}$$

TEST OF MODEL PERFORMANCE

A sample calculation is given in Fig. 10. The calculation is based on the second experimental run in Table 1 of Muto (2001), for which θ_{base} = 12.5°, $\dot{\xi}$ = 0.151 mm/s, q_{psf} = 0.904 cm^2/s and q_w = 4.36 cm^2/s. The shoreline initially prograded, or regressed. It next entered autoretreat, however, and began to slowly transgress. Eventually the sediment transport rate at the shoreline dropped to zero, and the shoreline commenced rapid sediment-starved autoretreat. The pattern of development was the same as that illustrated in Figs. 4 and 5.

The following parameters are chosen in order to compare the performance of the numerical model against all 29 runs of Table 1 of Muto (2001). The length of the fluvial topset at the end of the run L_{ae} is defined as

$$L_{ae} = s_s(t_{end}) - s_{ba}(t_{end}) \tag{37}$$

where t_{end} denotes the end run time. Let s_{auto} and t_{auto} denote the distance to the point at which autobreak occurs and the time of autobreak, respectively. The elevation of the autobreak point above the bedrock basement η_{ab} is given as

$$\eta_{ab} = \eta(s_{auto}, t_{auto}) - \eta_{base}(s_{auto}) \tag{38}$$

In Figs. 11, 12 and 13 computed values of L_{ae}, t_{auto} and η_{ab} are compared against measured values for all the runs of Table 1 of Muto (2001). While the agreement is by no means perfect, the numerical model captures the basic trends of the experiments without gross error. The discrepancies are most likely due to the inadequacies of the rather simple sediment transport formulation of (1), and in particular to the lack of a threshold condition for the transport of sediment therein.

CONCLUSIONS

In summary, the basic features of the experiments of Muto (2001) are captured by the moving boundary model. Most importantly, the model captures the transgressive autoretreat of the shoreline (topset-foreset break) driven by base level rise, including slow transgression with some sediment delivery to the delta front, autobreak, and subsequent rapid shoreline transgression and abandonment of the delta front. The numerical model is adapted to field conditions in Part II (Parker *et al*., submitted) and applied as a tool to study the effect to sea level rise on a large river in Papua New Guinea.

ACKNOWLEDGEMENTS

This paper includes material from a paper in a conference proceedings, Parker and Muto (2003); and its companion paper, Parker *et al*. (submitted) includes material from another paper in a conference proceedings, Parker *et al*. (2004). The scope of the work has been greatly extended in the present paper and its companion.

This research was funded by the National Science Foundation Source to Sink Program (Collaborative Research: Processes Controlling Depositional Signals of Environmental Change in the Fly River Sediment Dispersal System: Rates and Mechanisms of Floodplain Deposition, EAR-0203296) and the National Center for Earth-surface Dynamics (NCED), a National Science Foundation Science and Technology Center (EAR-0120914). This paper is a contribution of the research effort of NCED in the area of channel dynamics. The

participation of Y. Akamatsu was enabled by a grant from the Japan Society for the Promotion of Science.

REFERENCES

Bard, E., Hamelin, B., Arnold, M., Montaggioni, L., Cabioch, G., Faure, G. and **Rougerie, F.** (1996) Deglacial sea-level record from Tahiti corals and the timing of global meltwater discharge. *Nature*, 382, pp. 241-244.

Blum, M. B. and **Törnqvist, T. E.** (2000) Fluvial responses to climate and sea-level change: a review and look forward. *Sedimentology*, **47** (Suppl. 1), 2-48.

Bratton, J.F., Colman, S.M., Thieler, E.R. and **Seal, R.R.I.** 2003. Birth of the modern Chesapeake Bay estuary 7.4 to 8.2 ka and implications for global sea-level rise. *Geo-Marine Letters*, **22**, 188-197.

Brownlie, W. R. (1981) Prediction of flow depth and sediment discharge in open channels. *Report* No. KH-R-43A, W. M. Keck Laboratory of Hydraulics and Water Resources, California Institute of Technology, Pasadena, California, USA, 232 p.

Dietrich, W. E., Day, G. and **Parker, G.** (1999) The Fly River, Papua New Guinea: inferences about river dynamics, floodplain sedimentation and fate of sediment. In *Varieties of Fluvial Form*, Miller, A. J. and Gupta, A., eds., John Wiley and Sons, New York, 345-376.

Kostic, S., Parker, G. and **Marr, J.** (2002) Role of turbidity currents in setting the foreset slope of clinoforms prograding into standing fresh water. *Journal of Sedimentary Research*, **72(3)**, 353-362.

Kostic, S. and **Parker, G.** 2003a Progradational sand-mud deltas in lakes and reservoirs Part 1. Theory and numerical modeling. *Journal of Hydraulic Research*, **41(2)**, 127-140.

Kostic, S. and **Parker, G.** 2003b Progradational sand-mud deltas in lakes and reservoirs Part II. Experiment and numerical simulation. *Journal of Hydraulic Research*, **41(2)**, 141-152.

Muto, T. and **Steel, R. J.** (1992) Retreat of the front of a prograding delta. *Geology*, **20**, 967-970.

Muto, T. and **Steel, R. J.** (1997) Principles of regression and transgression: the nature of the interplay between accommodation and sediment supply. *Journal of Sedimentary Research*, **71**, 246-254.

Muto, T. (2001) Shoreline autoretreat substantiated in flume experiment. *Journal of Sedimentary Research*, **71(2)**, 246-254.

Muto, T. and **Steel, R. J.** (2001) Autostepping during the transgressive growth of deltas: Results from a flume experiment. *Geology*, **29(9)**, 771-774.

Paola, C. (2000) Quantitative models of sedimentary basin filling. *Sedimentology*, **47** (Suppl. 1), 121-179.

Parker, G. and **Muto, T.** (2003) 1D numerical model of delta response to rising sea level, *Proceedings*, 3rd IAHR Symposium, River, Coastal and Estuarine Morphodynamics, Barcelona, Spain, September 1-5., 10 p.

Parker, G., Akamatsu, Y., Muto, T. and **Dietrich, W. E.** (2004) Modeling the effect of rising sea level on river deltas and long profiles of rivers. *Proceedings*, International Conference on Civil and Environmental Engineering ICCEE-2004, Hiroshima University, Higashi-Hiroshima, Japan, July 27-28, 1-11.

Parker, G., Muto, T., Akamatsu, Y., Dietrich, W. E. (submitted) Unraveling the conundrum of river response to rising sea level from laboratory to field. Part II. The Fly-Strickland River System, Papua New Guinea. *Sedimentology.*

Swenson, J. B., Voller, V. R., Paola, C., Parker, G. and **Marr, J.** (2000) Fluvio-deltaic sedimentation: A generalized Stefan problem. *European Journal of Applied Math*., **11**, 433-452.

NOMENCLATURE

Symbol	Meaning	Dimensions (**L** length, **M** mass, **T** time, (1 dimensionless)
D	Characteristic (median or geometric mean) sediment grain size	**L**
i	Index denoting either the ith spatial node or the initial value of a parameter	1
L_{ae}	Length of the fluvial topset at run end in the experiments of Muto (2001)	**L**
N	Number of intervals in spatial discretization	1
q_{ps}	$= q_s/(1 - \lambda_p)$, volume sand transport rate per unit width including pores	$\mathbf{L^2T^{-1}}$
q_{psf}	Volume sand feed rate per unit width including pores	$\mathbf{L^2T^{-1}}$
q_{pss}	Value of q_{ps} at shoreline	$\mathbf{L^2T^{-1}}$
q_s	Volume sand transport rate per unit width excluding pores	$\mathbf{L^2T^{-1}}$
q_w	Water discharge per unit width	$\mathbf{L^2T^{-1}}$
R	$= (\rho_s/\rho - 1)$, submerged specific gravity of sediment (~ 1.65 for quartz)	1
S	$= - \partial\eta/\partial x$, local alluvial bed slope	1
S_{aba}	Alluvial slope at bedrock-alluvial transition	1
S_b	Constant basement slope of the experiments of Muto (2001)	1
S_{fi}	Initial slope of fluvial region	1
S_{fore}	Foreset slope (assumed constant here)	1
S_u	Alluvial bed slope at bedrock-alluvial transition	1
s_{auto}	Distance to the point where autobreak occurs in the experiments of Muto (2001)	**L**
s_{ba}	Position of bedrock-alluvial transition	**L**
$\dot{s}_{ba}$	Migration speed of bedrock-alluvial transition	$\mathbf{LT^{-1}}$
s_s	Position of shoreline	**L**
s_{si}	Initial value of s_s	**L**

$\dot{s}_s$	Migration speed of shoreline	$\mathbf{LT^{-1}}$
s_{sb}	Position of foreset-subaqueous basement break	**L**
s_{sbi}	Initial value of s_{sb}	**L**
$\dot{s}_{sb}$	Migration speed of foreset-subaqueous break	$\mathbf{LT^{-1}}$
t	Time	**T**
t_{auto}	Time to autobreak in experiment of Muto (2001)	**T**
t_{end}	Time of end of run in experiments of Muto (2001)	**T**
$\bar{t}$	Moving boundary time coordinate given by (21b)	**T**
x	Downchannel streamwise coordinate	**L**
$\bar{x}$	Dimensionless moving boundary spatial coordinate given by (21a)	1
$\Delta\bar{x}$	Interval length in discretization of $\bar{x}$	1
$\Delta\bar{t}$	Step length in time $\bar{t}$	**T**
$\Delta\eta$	Elevation drop across the foreset	**L**
$\Delta\eta_i$	Initial value of $\Delta\eta$	**L**
η	Local alluvial bed elevation	**L**
η_{ab}	Elevation of the autobreak point above basement at time of autobreak in experiments of Muto (2001)	**L**
η_{bi}	Initial elevation of the foreset-subaqueous basement break	**L**
η_{base}	Local basement elevation	**L**
η_s	Bed elevation at the shoreline	**L**
λ_p	Porosity of deposit	1
θ_{base}	Angle of inclination of basement slope experiments of Muto (2001)	1 (radians or degrees)
θ_r	Angle of repose of sediment	1 (radians or degrees)
θ_u	Alluvial bed slope angle at bedrock-alluvial transition	1 (radians or degrees)
ρ	Density of water	$\mathbf{ML^{-3}}$
ρ_s	Density of sediment	$\mathbf{ML^{-3}}$
ξ	Sea level or elevation of standing water (base level)	**L**
ξ_i	Initial value of ξ	**L**
$\dot{\xi}$	Rate of rise of sea level or elevation of standing water	$\mathbf{LT^{-1}}$

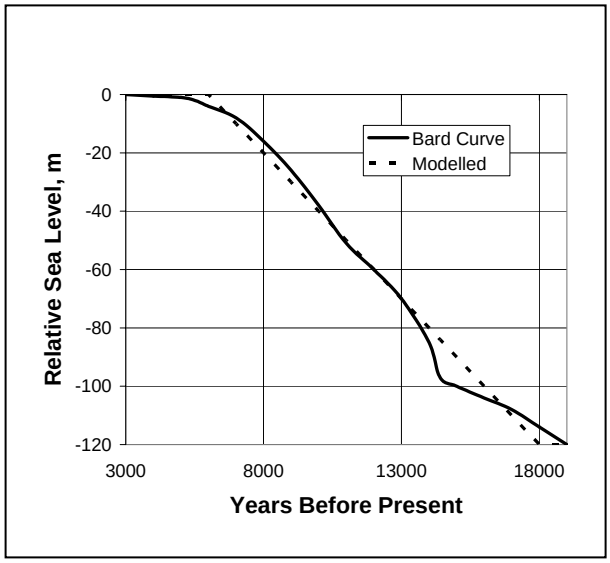

Figure 1. The solid line (Bard Curve) denotes a simplified version of the curve of eustatic sea level relative to present-day conditions presented by Bard *et al*. (1996). The dashed line denotes the curve used in two applications of the numerical model, i.e. Cases B and C, with a constant sea level rise of 10 mm/a for 12000 years.

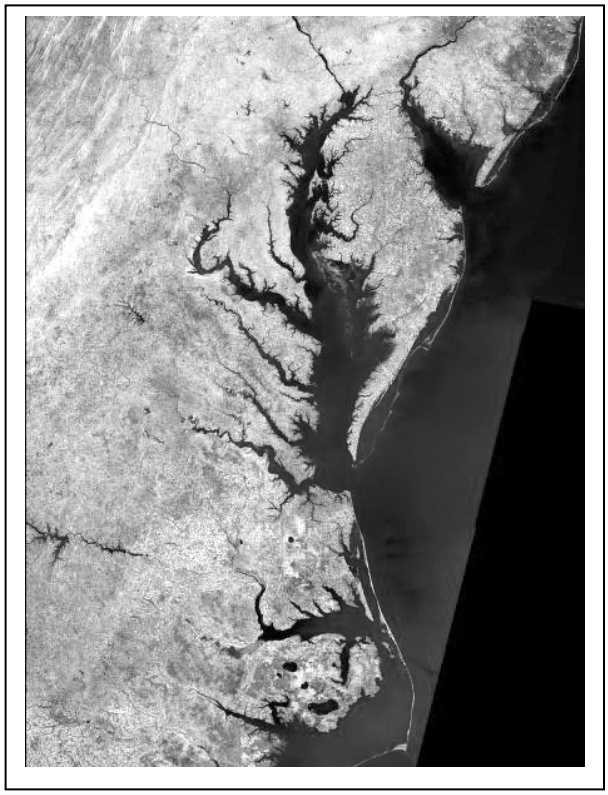

Figure 2. Satellite view of the Eastern Seaboard of the United States from Albemarle Sound (bottom, south) to Delaware Bay and New Jersey (top, north).

The image is from the NASA web site, https://zulu.ssc.nasa.gov/mrsid/. Note the presence of numerous drowned river valleys.

Figure 3. Satellite image of the Mississippi River delta. Image from NASA. Note how the Mississippi Delta protrudes into the Gulf of Mexico.

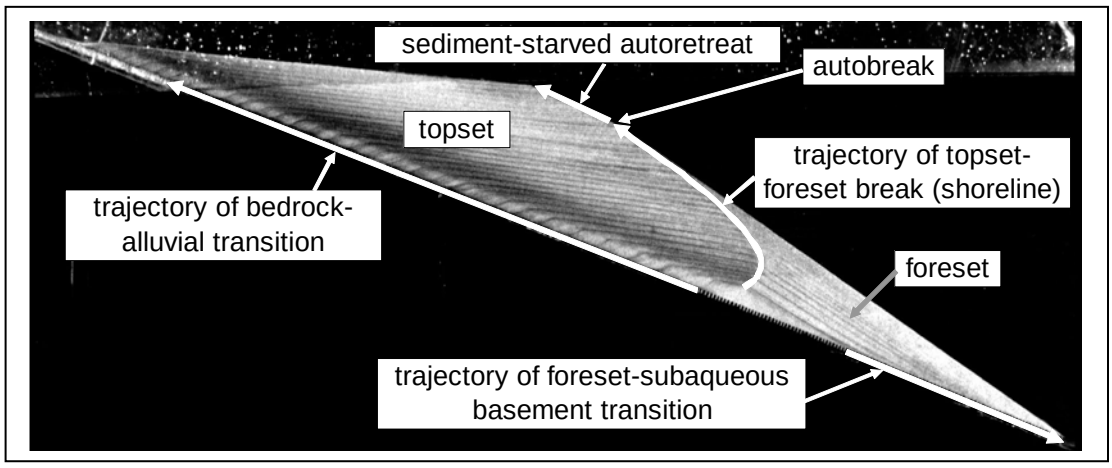

Figure 4. Annotated image from the end of one of the experiments of Muto (2001). Flow was from left to right.

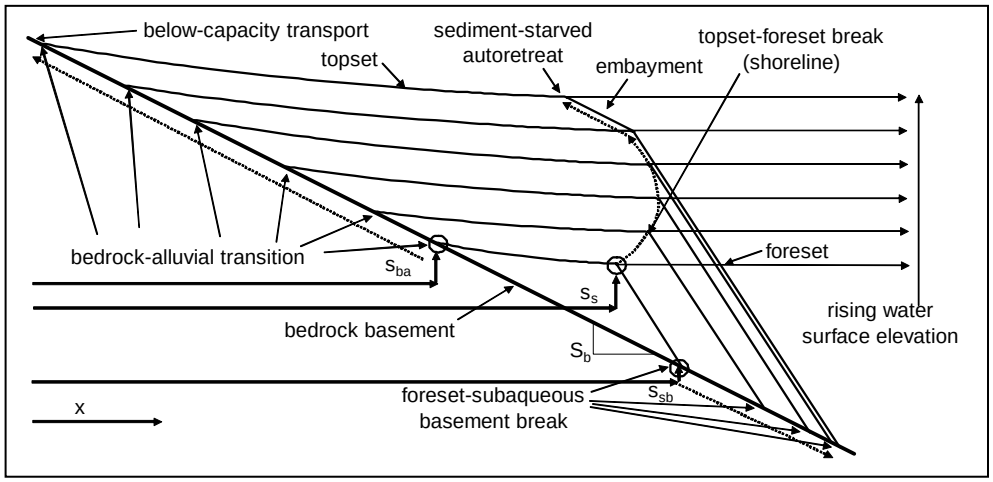

Figure 5. Sketch of delta evolution observed by Muto (2001) under conditions of rising sea level

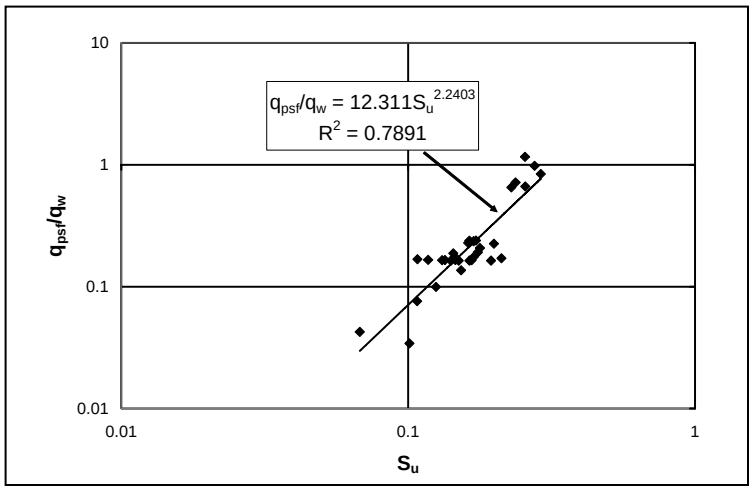

Figure 6. Sediment transport relation determined empirically from the experiments of Muto (2001).

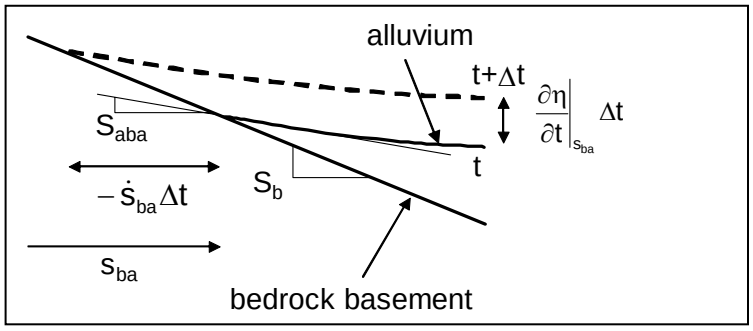

Figure 7. Diagram illustrating continuity condition at the bedrock-alluvial transition.

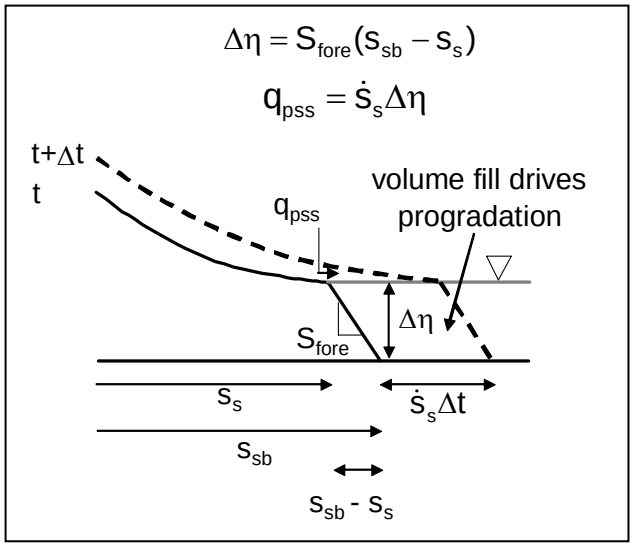

Figure 8a. Illustration of delta evolution over a horizontal subaqueous basement and with constant base level.

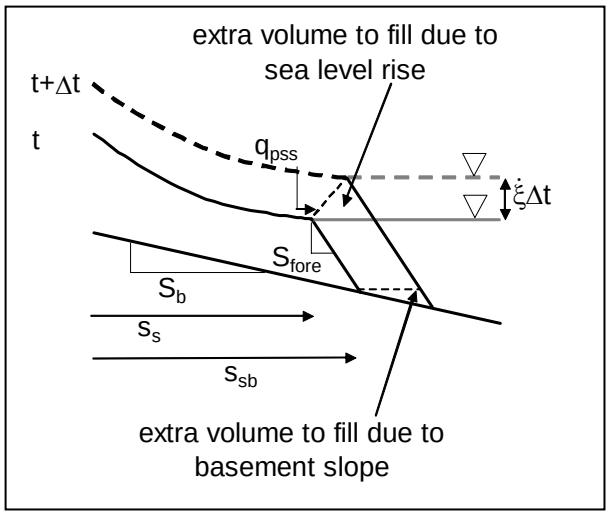

Figure 8b. Illustration of delta evolution as it progrades over a seaward-sloping subaqueous basement, and with rising sea level. Both features act to slow down delta progradation.

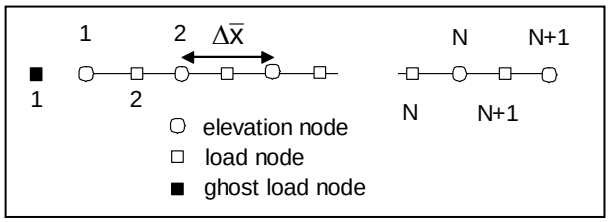

Figure 9. Illustration of the grid used in the numerical model of the experiments of Muto (2001).

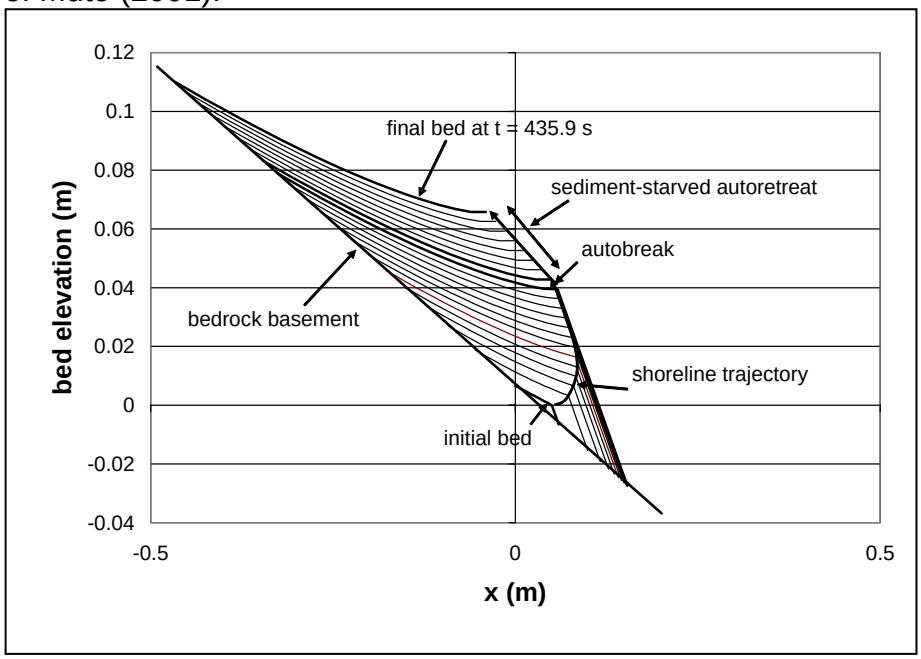

Figure 10. Sample numerical results based on an experiment of Muto (2001) for which θ_{base} = 12.5°, $\dot{\xi}$ = 0.151 mm/s, q_{psf} = 0.904 cm^2/s and q_w = 4.36 cm^2/s

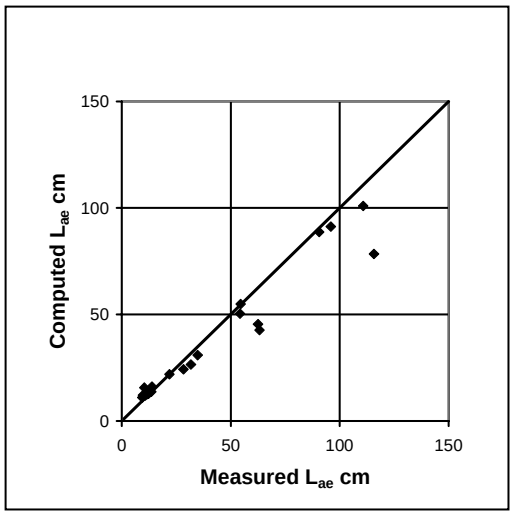

Figure 11. Comparison of computed versus measured values of L_{ae}, where L_{ae} denotes the length of the alluvial reach from bedrock-alluvial transition to shoreline at the end of the run, for the experiments of Muto (2001)

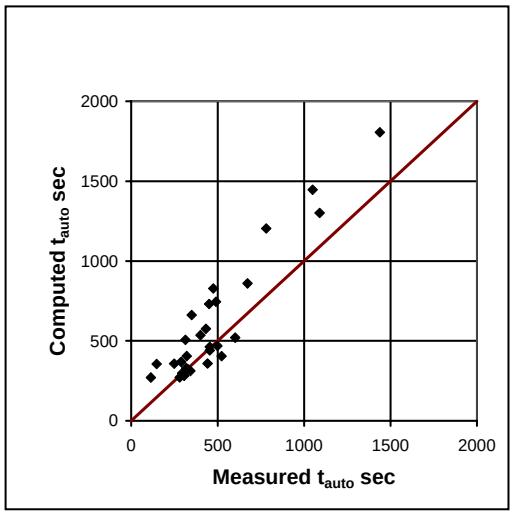

Figure 12. Comparison of computed versus measured time to autobreak t_{auto} for the experiment of Muto (2001).

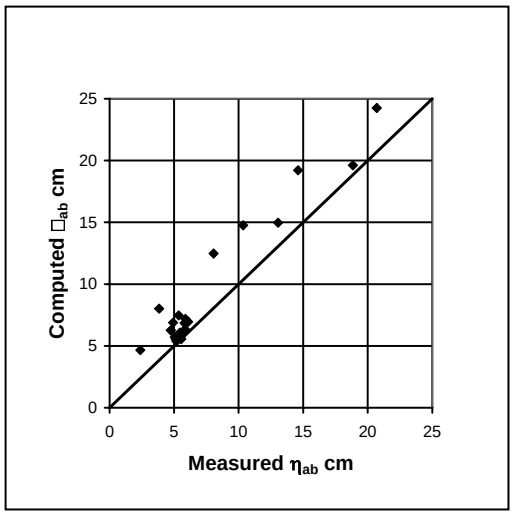

Figure 13. Comparison of computed versus measured values of η_{ab} for the experiments of Muto (2001), where η_{ab} denotes the elevation of the topset-foreset break (shoreline) above the bedrock basement at the end of the run.
ect of river scale.